Accepted Manuscript

Title: Photodegradation of herbicide Metsulfuron-methyl with TiO_2 supported on magnetite particles coated with SiO_2

Authors: Juan Paulo Montañez, Carla Lorena Heredia, Edgardo Ling Sham, Elsa Mónica Farfán Torres

PII: S2213-3437(18)30386-5
DOI: https://doi.org/10.1016/j.jece.2018.07.006
Reference: JECE 2501

To appear in:

Received date: 27-4-2018
Revised date: 13-6-2018
Accepted date: 3-7-2018

Please cite this article as: Montañez JP, Heredia CL, Sham EL, Torres EMF, Photodegradation of herbicide Metsulfuron-methyl with TiO_2 supported on magnetite particles coated with SiO_2, *Journal of Environmental Chemical Engineering* (2018), https://doi.org/10.1016/j.jece.2018.07.006

Photodegradation of herbicide Metsulfuron-methyl with TiO_2 supported on magnetite particles coated with SiO_2

Juan Paulo Montañez[a,*], Carla Lorena Heredia[b], Edgardo Ling Sham[c], Elsa Mónica Farfán Torres[b]

[a] *Instituto de Investigaciones para la Industria Química, Universidad Nacional de Salta, CONICET, 4400, Salta, Argentina.*
[b] *Instituto de Investigaciones para la Industria Química, Universidad Nacional de Salta, CONICET, FCE, 4400, Salta, Argentina.*
[c] *Instituto de Investigaciones para la Industria Química, Universidad Nacional de Salta, CONICET, FI, 4400, Salta, Argentina.*
*Corresponding author at: Instituto de Investigaciones para la Industria Química, Universidad Nacional de Salta, Avenida Bolivia 5150, 4400, Salta, Argentina. E-mail address: jpm_27ar@yahoo.com.ar

Abstract
Natural watercourses may be significantly contaminated due to the increase of agricultural activities, making it necessary to develop new methodologies for the remediation of agrochemicals, including herbicides. To this effect, photodegradation with TiO_2 is a very effective process. However, this semiconductor cannot be easily removed from the treated aqueous medium. Supporting the photocatalyst on different materials facilitates its removal by several methods, including magnetic attraction. According to this goal, this work reports the synthesis of TiO_2 photocatalysts supported on SiO_2-coated magnetite particles (Fe_3O_4) by a low-temperature sol-gel process (75 °C). By varying the aging time of the TiO_2 sol, materials with different structural properties and combinations of anatase-brookite phases were obtained. Of all the synthesized solids, the one with the highest photocatalytic activity in the degradation of model compounds was the $TiO_2/SiO_2/Fe_3O_4$ catalyst with a 47.4/13.6/39.0 wt % respectively. Under optimal working conditions and at a pH value close to neutrality (conditions in which Metsulfuron-methyl is persistent in an aqueous medium) this catalyst degraded 70% of the herbicide initial concentration in three and a half hours of artificial irradiation with an activity similar to the mass TiO_2. The aging time significantly influenced on structural properties of supported TiO_2. With its increase, the degree of crystallinity of the samples also increased but its specific surface decreased. The catalyst with higher photoactivity blends the best combination of both factors and is, therefore, a good alternative for the remediation of contaminated effluents with commercial formulations of this herbicide. Also, its magnetic support facilitates its subsequent removal from treated water samples.

Keywords supported catalysts, TiO_2, photodegradation, remediation.

1. Introduction

Heterogeneous photocatalysis with TiO_2 is a widely used process in the degradation of contaminants present in aqueous effluents of domestic, industrial or agricultural sources [1]. However, this semiconductor cannot be easily removed due to the small size of its particles and remains in suspension once the reaction is complete and therefore costly separation methods are necessary. In addition, if these nanoparticles are released to natural watercourses, they can cause serious damage to aquatic organisms [2] and humans [3].

To avoid this problem TiO_2 can be supported on a material that facilitates its further elimination, for example, magnetite (Fe_3O_4) [4]. By applying an external magnetic field to this kind of solids, it can be completely removed from the reaction medium. However, several investigations have shown that the direct deposition of TiO_2 on magnetite reduces considerably its photocatalytic properties. The heat treatment, necessary to transform the supported TiO_2 to active phases, produces the migration of Fe^{3+} ions to the TiO_2 lattice thus forming pseudobrookite (Fe_2TiO_5) [5], and oxidation of magnetite to species with less magnetic susceptibility [6], affecting its ability to magnetic separation. Also, the magnetic core may act as electron-hole recombination center [7] and besides photo-dissolution of Fe may take place [7a] in irradiation experiments thus affecting the whole photocatalytic process. To protect the catalytic activity of TiO_2 it is necessary to coat the Fe_3O_4 with another more inert oxide, being SiO_2 the most used for this purpose. SiO_2 act as a protective barrier between Fe_3O_4 and TiO_2, and also improves its photocatalytic performance [5, 8,9, 7c]. Based on these observations, some methodologies have been proposed to obtain anatase at low temperature (T <100 °C), including hydrothermal treatment [10], calcination in an N_2 atmosphere to avoid the presence of oxygen [8] or other modifications in the TiO_2 synthesis procedure [11]. Xu et al. synthesized anatase by aging TiO_2 sol at 75 °C for 24 h. Further, these particles were deposited onto magnetite cores (with and without SiO_2 shell) and its photocatalytic activities were investigated using phenol as a model compound [9]. Also, they used this synthesis procedure to deposit anatase particles on activated carbon obtaining a good photocatalytic response on phenol degradation, with an activity stable enough to allow the reuse of the photocatalyst [12]. However, the influence of TiO_2 sol aging time on the structural characteristics of this semiconductor has not yet been evaluated, to our knowledge.

In this work, we report the synthesis of TiO_2 supported on SiO_2-coated magnetite particles at 75 ºC. We have investigated different aging times of the TiO_2 sol in order to evaluate the influence of this variable on the formation of

crystalline phases and consequently on their catalytic behavior. The activity of the supported catalysts has been first evaluated in the degradation of tartrazine as a model compound. Once the best active catalyst was selected, its efficacy in the degradation of the Metsulfuron-methyl herbicide contained in a commercial formulation under different reaction conditions was investigated. Its behavior was compared with mass (synthesized and commercial) TiO_2, also comparing the use of artificial irradiation with the results obtained with solar irradiation. Our objective was to evaluate the factors that influence the photocatalytic degradation of this herbicide in order to find the best conditions for its application, thus achieving a process with feasibility of application in real working conditions.

2. Experimental section

2.1 Reagents

Supported catalysts were synthesized using the following reactants: Tetraethyl orthosilicate (TEOS, Merck), anhydrous ethanol (Biopack), ammonium hydroxide 28% m/v (Cicarelli), magnetite (Alfa Aesar), Titanium (IV) isopropoxide 97% (TIP, Aldrich), nitric acid (Anedra) and distilled water. Tartrazine was supplied by Sigma-Aldrich and used as received. Metsulfuron-methyl 60 WG-DVA and TiO_2 P25 were kindly supplied by Belagro and Evonik Argentina, respectively.

2.2 Synthesis of SiO_2-coated magnetite particles (FS)

1.00 g Fe_3O_4 was added to a mixture of 40 mL ethanol, 1 mL distilled water, 4 mL NH_4OH and 3 mL TEOS. This mixture was continuously stirred at room temperature for 6 h. The resulting particles were magnetically sedimented, washed repeatedly with distilled water and dried in an oven at 80 ºC overnight.

2.3 Synthesis of TiO_2 supported on FS (FST photocatalysts)

10 mL TIP 1 mol L^{-1} solution (isopropyl alcohol as solvent) were added dropwise to 20 mL distilled water at pH 2 under continuous stirring. This mixture was heated at 75 ºC under reflux conditions at different aging times: 2.5, 5, 16, 24 and 72 h.

At the end of aging time, 0.5 g FS were added to TiO_2 sol and this mixture was sonicated at room temperature for 1 h. The secondary products were eliminated by rotary evaporator at 80 ºC. Finally, the as-prepared magnetic catalysts were washed with distilled water and dried in an oven at 80 ºC overnight. These composites were denominated FST-2.5, FST-5, FST-16, FST-24 and FST-72, according to its aging time.

2.4 Characterizations

FT-IR and Raman spectra of the solids were obtained on a GX Perkin Elmer spectrometer. Due to instrumental limitations to characterize dark solids by Raman spectroscopy, unsupported TiO_2 samples with different aging times were analyzed as pure phase. Differential Thermal Analysis (DTA) and Thermogravimetric Analysis (TGA) were performed on a Rigaku TAS 1100 analyzer in static air at a heating rate of 20°C min^{-1}. Nitrogen adsorption-desorption analysis was carried out at 77 K on a Micromeritics ASAP 2020 adsorption analyzer. XRD patterns were acquired on a Bruker AXS D8 diffractometer using CuK_α radiation in the range of 2θ = 20 – 60°. Scanning electron microscope (SEM) images were obtained using a JEOL JSM-6480LV microscope equipped with a Thermo Electron NORAN System SIX energy dispersive X-ray spectroscopy (EDS) analyzer. The composition of solids was determined by EDS. Zero potentials were obtained by Z-Meter 3.0 equipment.

2.5 Photocatalytic reactions

The photocatalytic activity of the FST samples was evaluated on the degradation of tartrazine (a yellow azo dye) and Metsulfuron-methyl (a sulfonylurea herbicide) on 500 mL solutions with starting concentrations of 2 x 10^{-5} mol L^{-1} each. The catalyst concentrations ranged from 0.1 g L^{-1} to 3.0 g L^{-1}. Prior to irradiation, the suspensions were mechanically stirred for 20 min to establish the adsorption/desorption equilibrium between the photocatalyst and the compound to be degraded. All experiments were performed in duplicate on an opened cylindric glass reactor with mechanical stirring and upper irradiation with an Osram Ultra-Vitalux 300 W lamp. The emission intervals and intensities of this lamp are, according to the manufacturer's specifications: UVB (280-315 nm) 2.2 W m^{-2}; UVA (315-400 nm) 5.1 W m^{-2}; visible range (400-780 nm) 12 W m^{-2}. Aliquots were withdrawn at specific time intervals and catalyst particles were removed by a magnet (magnetic supported catalysts) or 0.20 µm Sartorius cellulose acetate membranes (unsupported TiO_2). GBC Cintra 10E double beam UV–vis spectrometer was employed to determine the degradation efficiency of tartrazine and Metsulfuron-methyl at λ = 427 nm and λ = 232 nm respectively. Concentrated NaOH solutions were employed to adjust initial pH of herbicide solutions.

For catalysts reuse experiments, the magnetically-recovered catalyst was only rinsed with plenty of distilled water and immediately reused with a new herbicide solution.

3. Results and discussion

3.1 IR and Raman spectra

Figure 1 shows FTIR spectrum of FS. The characteristic bands of Fe_3O_4 at 584 and 634 cm^{-1} belongs to Fe–O bond. Asymmetrical stretching of Si–O–Si structure can be seen at 1098 and 1200 cm^{-1} [13]. Absorption bands at 960 and 800 cm^{-1} belongs to Si–O–H vibration and Si–O–Si symmetrical stretching respectively. Also, the band around 560 cm^{-1} is possibly due to vibration caused by perturbation of the metal ion in the tetrahedral SiO_4 [14].

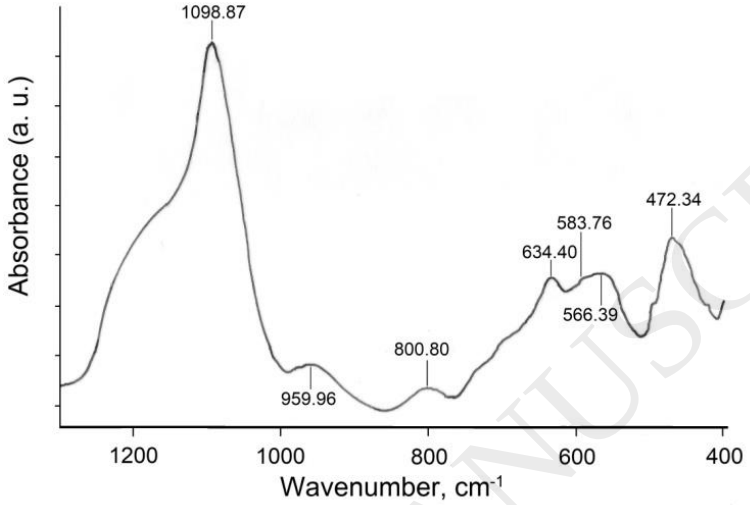

Fig. 1. FTIR spectrum of magnetic support FS.

Raman spectra of unsupported TiO_2-2.5 and TiO_2-5 (2.5 and 5 h aging time respectively) are shown in Figure 2. Three strong absorption bands are observed at 638, 516 and 398 cm^{-1} for TiO_2-5, which correspond to Eg, A_{1g}-B_{1g} and B_{1g} characteristic modes of the anatase phase respectively [15,16]. Weak bands at 323 and 443 cm^{-1} corresponding to brookite and rutile phase respectively can also be observed [16]. Raman spectra of TiO_2-16, TiO_2-24 and TiO_2-72 are identical to TiO_2-5 spectrum, and therefore, are not presented in Figure 2.

The same bands above mentioned can be seen in the TiO_2-2.5 spectrum but they are wider and of lower-intensity. These bands correspond to the presence of Ti (TiO_6^{2-}) octahedrally coordinated at short range. The wide band at 410 cm^{-1} probably corresponds to a peaks superposition of both anatase and brookite phases [16]. Also, two bands at 443 and 611 cm^{-1} indicate the incipient formation of the rutile phase.

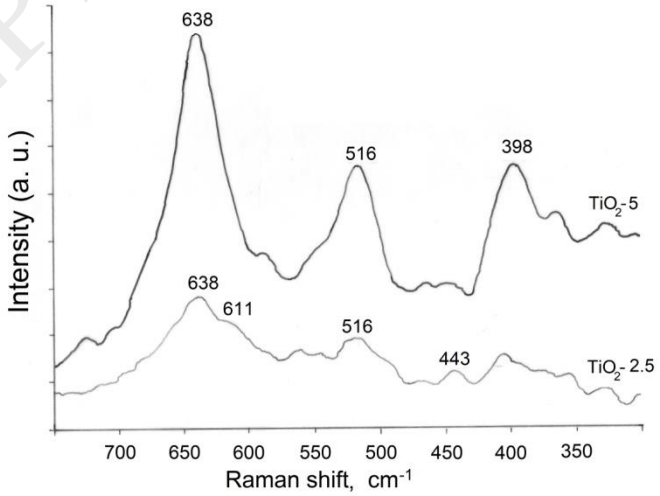

Fig. 2. Raman spectra of unsupported TiO_2-2.5 and TiO_2-5 (2.5 and 5 h aging time respectively).

Gopal et al. [17] established an approximate phase transformation diagram for TiO_2 as a function of temperature. This diagram shows that both anatase and rutile phase can be formed at low temperature (T ≤ 100°C) and that it is possible that they exist together under specific conditions of heating rate and the aging time used at the final temperature.

In this work all samples were synthesized at same heating rate, thus aging time was the main factor that determines the predominant formation of anatase phase in these solids.

3.2 Thermal Analysis

Figure 3 shows DTA and TGA curves of Fe_3O_4 (a) and supported TiO_2 samples (b-e) prepared at different aging time. On TGA curve of Fe_3O_4 it can be seen a slight mass increase (ca. 0.6%) up to 340 ºC, due to oxidation of magnetite phase to maghemite phase ($Fe^{2+}O.Fe_2^{3+}O_3 \rightarrow \gamma$-$Fe_2O_3$) [18,19].This fact is related to the first exothermic event in the DTA curve of magnetite at the same temperature, while the second peak at 650 ºC indicates conversion to hematite phase (α - Fe_2O_3) without any mass change [19].

All TGA curves on Figure 3 (b - e) show similar characteristics and they present three well-differentiated slopes with 13.5% average total mass loss. TG/DTA curves of TiO_2-2.5 are identical to those of TiO_2-5 curves, and therefore, are not presented in Figure 3. Elimination of physisorbed water molecules on TiO_2 (ca. 7%) occur from 100 to 150 ºC. Up to 300 °C, the partial oxidation of alkyl groups associated with TiO_2 synthesis takes place. Finally, in the temperature range of 300 to 500 °C 1.5% of the mass is lost, possibly due to combustion of some organic residues coming from TiO_2 synthesis.

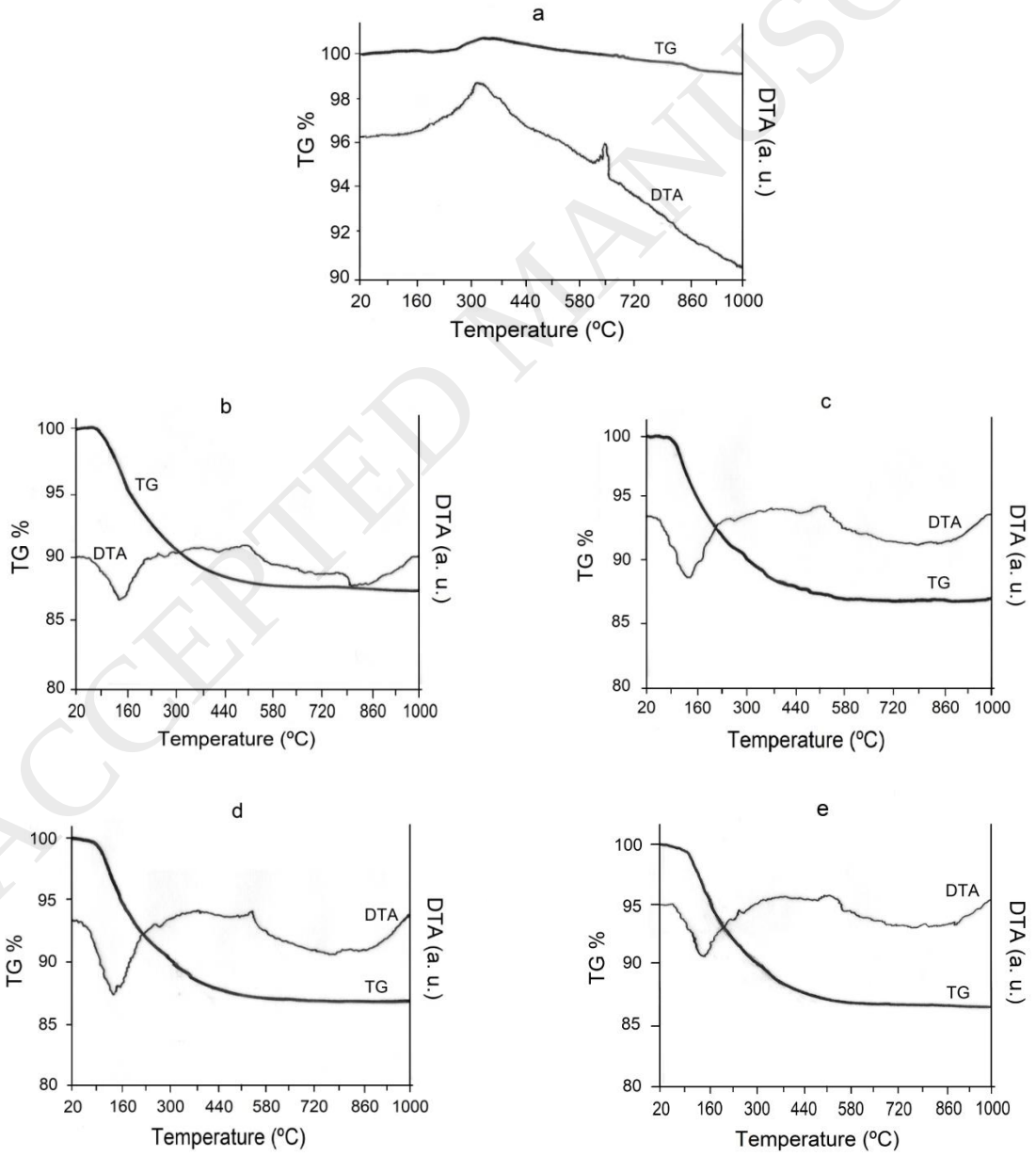

Fig. 3. DTA and TGA curves of (a) Fe_3O_4, (b) TiO_2 - 5, (c) TiO_2 - 16, (d) TiO_2 - 24 and (e) TiO_2 – 72. Curves (b-e) belong to synthesized TiO_2 with aging time of 5, 16, 24 and 72 h respectively.

DTA curves of solids show similar characteristic between them, with three main events. At 130ºC takes place an endothermic event due to the loss of water as indicated above for the TGA curves [20]. The second event, an exothermic one, corresponds to a little peak at 230 ºC related to the thermooxidative degradation of remanent organic matter [20]. The last exothermic event at 540 ºC can be associated with anatase-rutile phase transitions [21,22]. These phase changes do not involve significant variation in mass. This whole process produced the densification of the heat-treated sample, which involves a decrease in pore volume and surface area.

3.3 Surface area

Table 1 shows the specific surface area, micro-and mesopore volumes of synthesized solids. Magnetite particles coated with SiO_2 and TiO_2 have larger specific surface area than bare magnetite particles, and FST-2.5 has the largest of all solids. As can be seen, the increase of aging time reduces the surface area. The volumes of micro- and mesopores of photocatalysts presented in Table 1 were calculated from the corresponding isotherms (type IV, irreversible and H3 type hysteresis cycle). The found values follow the same trend as the specific surface: the volume of mesopores decreases gradually as the aging time increases.

Table 1 Specific surface areas, meso- and micropore volume of solids.

Sample	Aging Time (h)	Specific Surface (m^2g^{-1})	Mesopore Volume ($cm^3\ g^{-1}$)	Micropore Volume ($cm^3\ g^{-1}$)
Fe_3O_4	-	7.4	-	-
FS	-	42	-	-
FST-2.5	2.5	201	0.25	0.02
FST-5	5	188	0.22	0.02
FST-16	16	178	0.19	0.02
FST-24	24	172	0.18	0.02
FST-72	72	135	0.15	0.01

3.4 XRD Analysis

Figure 4 shows characteristics diffraction peaks of Fe_3O_4 a 2θ = 30.1º, 35.5º, 37.0°, 43.1º, 53.5° and 57.0º, corresponding to cubic-spinel phase (AMCSD 945). XRD pattern of FS is similar to that of Fe_3O_4 with an additional wide band in the range of 2θ = 20 – 28°. This band corresponds to an amorphous silica phase which suggests that the magnetite particles are probably encapsulated [11b].

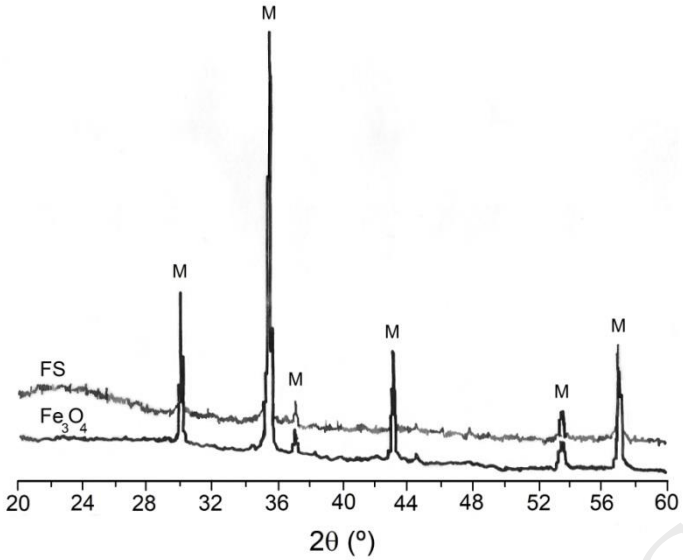

Fig. 4. XRD patterns of Fe_3O_4 and FS.
M letter indicates peaks corresponding to magnetite.

The diffractograms of FST-5, FST-16, FST-24 and FST-72 photocatalysts are very similar between them (Figure 5). It can be observed that the characteristic peaks of the magnetite phase are present and new bands are added, corresponding to anatase at 2θ = 25.5°, 38.2°, 48.1° and 54.5° [15], while the diffraction peak of rutile at 2θ = 44.2º is barely visible. On the other hand, the peak corresponding to brookite phase (2θ = 30.7°) is not noticeable because the peak of magnetite overlap with it.

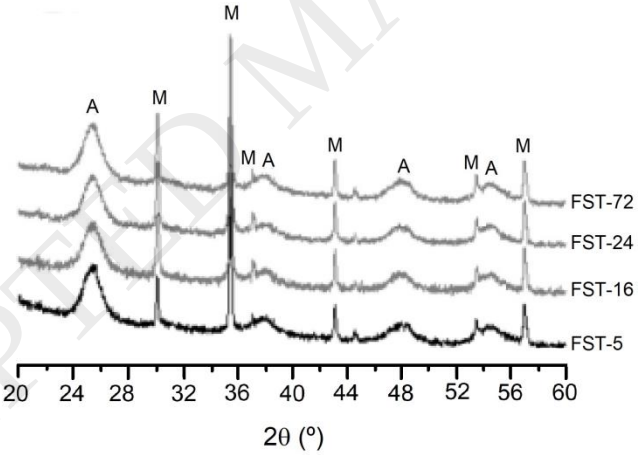

Fig. 5. XRD patterns of FST-5, FST-16, FST-24 and FST-72 photocatalysts.
A and M letters indicate peaks corresponding to anatase and magnetite respectively.

Figure 6 shows the diffraction patterns of unsupported TiO_2 at different aging time in order to analyze in detail the anatase, brookite and rutile phases that compose it. Anatase is the predominant phase in all samples as indicated by diffraction peaks at 2θ = 25.5°, 38.2°, 48.1° and 54.5° corresponding to (101), (004), (200) and (106) planes respectively (AMCSD 19093). Another low-intensity diffraction band appears at 2θ = 30.7º and is characteristic of the plane (121) of the brookite phase (AMCSD 5160). All these diffraction lines are consistent with the Raman spectra of the TiO_2-2.5 and TiO_2-5 samples on Figure 2.

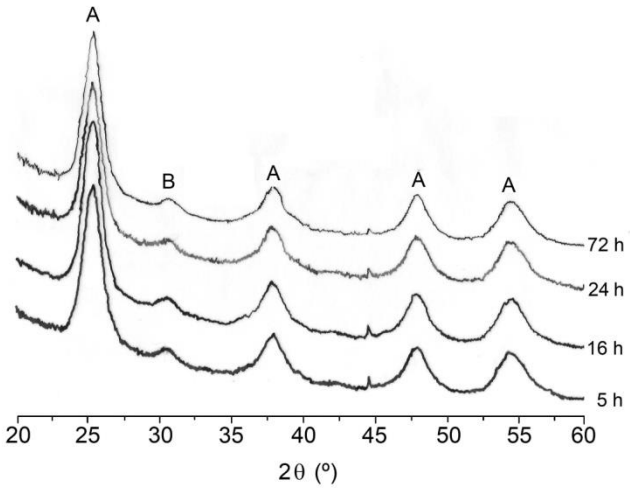

Fig. 6. XRD patterns of unsupported TiO_2 aged at 5, 16, 24 and 72 h.
A and B letters indicate peaks corresponding to anatase and brookite phases respectively.

Average particle sizes were determined by the Scherrer equation with peaks at 2θ = 25.5° for anatase and 2θ = 30.7° for brookite. These results are presented in Table 2.

Although the intensity of the diffraction peak of brookite is lower than that of anatase (broad peaks leads to particle sizes with significant error), this calculation allows to evaluate the development of both phases as the aging time elapses. The content of anatase (Ac) and brookite (Bc) of solids was calculated according to Zhang and Banfield method [23] using the above-mentioned peaks. There is a slight increase in the average size of the anatase crystallites as the aging time increases. In the brookite crystals, the same variation was observed except for the crystal obtained with a longer aging time (72 h). The latter value could present a greater error because the peak at 2θ = 30.7º is too wide. However, these values are consistent with the decrease in the specific surface area of the catalysts shown in Table 1.

Table 2 Crystallite size, anatase (Ac) and brookite (Bc) content of unsupported TiO_2

Sample	Anatase Crystal size (nm)	Brookite Crystal size (nm)	Ac (wt.%)	Bc (wt.%)
TiO_2-5	8.9	6.2	71.1	28.9
TiO_2-16	9.3	6.6	69.9	30.1
TiO_2-24	9.5	7.1	65.3	34.7
TiO_2-72	10.0	5.8	50.0	50.0

It was observed that the increase in the aging time produces a decrease in the proportion of anatase phase and increased that of brookite. Zhang and Banfield [23] found that phase transformation of TiO_2 depends strongly on particle size because the activation energies between phases are very close at nanometric sizes. When the size of primary crystals is less than 11 nm the thermodynamically favorable phase is anatase. For sizes between 11 and 35 nm the formation of the brookite phase is favored and above 35 nm the predominant development of rutile phase takes place [23]. Table 2 indicates that the predominant phase for the prepared solids is the anatase phase; when the particle size reaches 10 nm, the fraction of the brookite phase increases. Due to the fact that crystallization degree of this phase is low, its characteristic diffraction line is wide as shown in Figure 6.

Mutuma et al. [24] obtained TiO_2 crystals with anatase-brookite and anatase-brookite-rutile phases under different pH and temperature conditions. On samples synthesized at pH 2 (same value of our work), the rutile phase was only observed when the calcination temperatures were higher than 200°C. In our work all samples were synthesized at low temperature (75°C), thus this factor was determinant so that the rutile phase did not develop. The peak corresponding to rutile is barely perceptible in the Raman spectrum of Figure 2, confirming the control of temperature in the formation of phases.

3.5 SEM and EDS analyses

SEM images at 1000 and 3000x of magnetite particles are shown in Figure 7. These particles have a homogeneous size distribution with some small agglomerates.

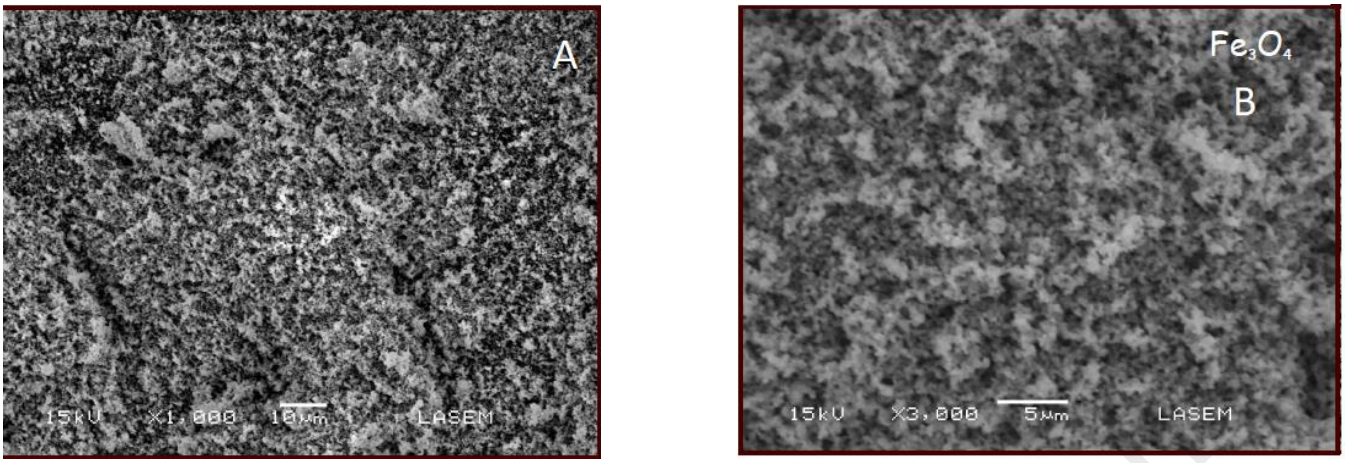

Fig. 7. SEM micrographs of Fe_3O_4 at 1000 (A) and 3000x (B).

Figure 8 shows FS particles. In general, a distribution quite similar to the uncoated Fe_3O_4 particles is observed and the agglomerates formed have a slightly larger size.

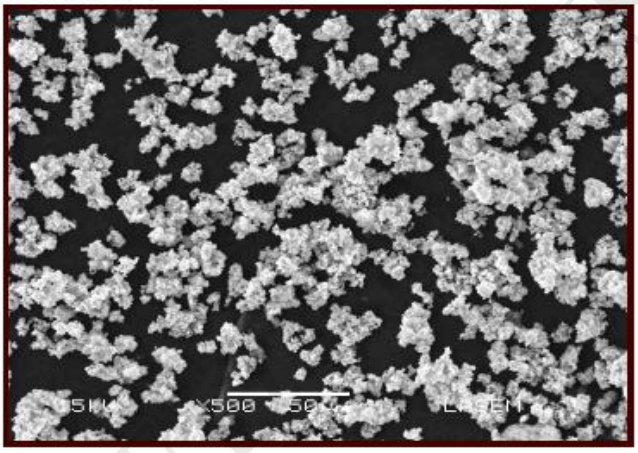

Fe3O4

Fig. 8. SEM micrograph of FS at 500x.

Figure 9 shows the micrographs of the FST-5 to FST-72 photocatalysts. As can be seen, morphology appears very similar between the different samples in all cases, with the formation of small agglomerates.

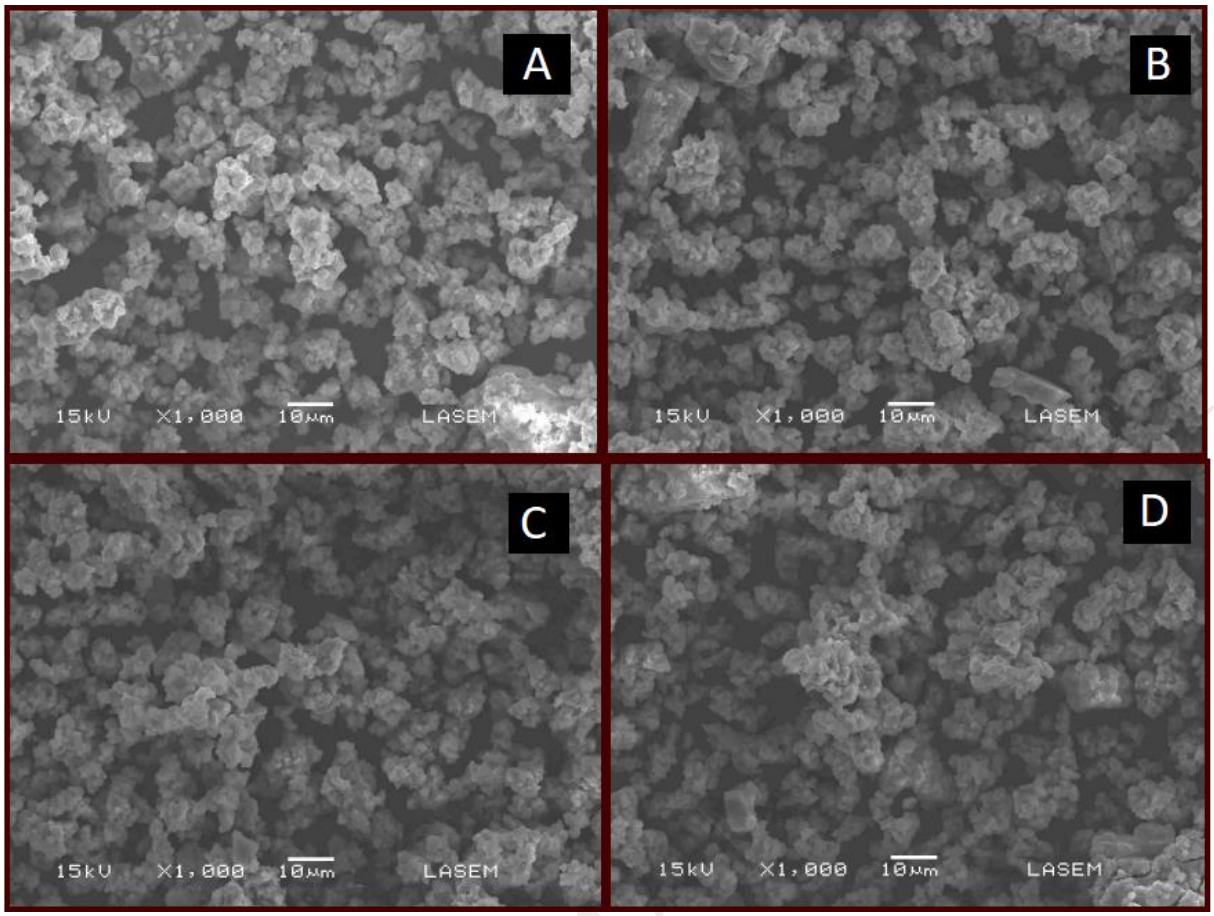

Fig. 9. SEM micrographs of FST-5 (A), FST-16 (B), FST-24 (C) and FST-72 (D) photocatalysts at 1000x.

Table 3 shows the chemical composition of the photocatalysts, determined by EDS. As can be seen, the amount of supported TiO_2 increases as the aging time increases. Initially, the primary crystallites are small and rearranged around the magnetic core FS. Then these crystals grow and more TiO_2 is deposited as the aging time increases. These results are in good agreement with results previously showed in Table 2.

Table 3 Chemical composition of photocatalysts by EDS.

Sample	Fe_3O_4 (wt.%)	SiO_2 (wt.%)	TiO_2 (wt.%)
FST-2.5	42.8	14.2	43.0
FST- 5	39.0	13.6	47.4
FST-16	39.7	10.4	49.9
FST-24	38.5	8.1	53.4
FST-72	36.2	6.3	57.5

3.6 Photocatalytic activity

3.6.1 Photodegradation of tartrazine as a model compound

Figure 10 shows the photocatalytic degradation of tartrazine as a model compound with the catalysts and FS nuclei. This magnetic support has no activity. FST-5 is the most active of all catalysts evaluated since it completely degrades the dye in 120 min of reaction. The photoactivity of the remaining catalysts decreases with the increase of the aging time used for its synthesis (FST-16, FST-24 and FST-72) or its low degree of crystallinity (FST-2.5).

The first of mentioned factors is related to the decrease of the specific surface of these three catalysts, as shown in Table 1. On the other hand, FST-2.5 does not present the adequate crystalline structure to promote the photocatalytic process although it possesses the highest specific surface area of all samples.

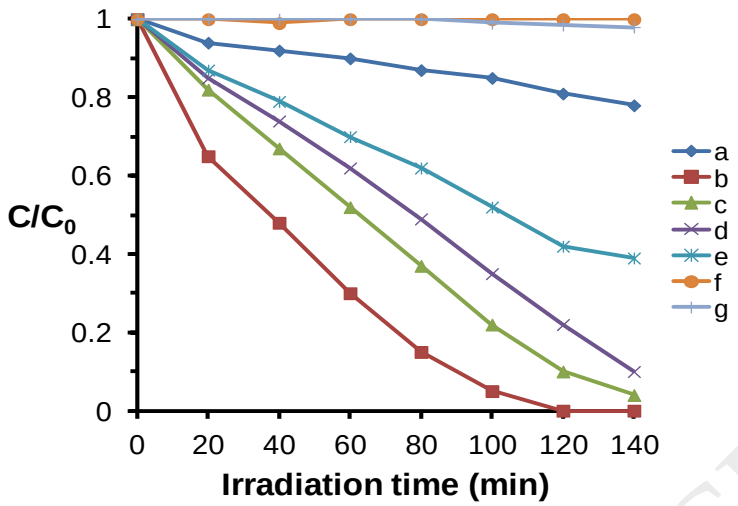

Fig. 10. Photocatalytic decomposition of tartrazine over (a) FST-2.5, (b) FST-5, (c) FST-16, (d) FST-24, (e) FST-72 catalysts and (f) magnetic nuclei FS at 0.1 g L^{-1} for all catalysts. Photolysis (g) is also shows.

The presence of different phases on a semiconductor improves its photoactivity since it leads to more efficient separation of the electron-hole pair. FST-5, composed of anatase-brookite, is a good example of this. Some authors have indicated that this phase composition was more effective than P25 (composed of anatase-rutile) in the degradation of some compounds such as methyl orange, methylene blue, rhodamine B, phenol, salicylic acid, acetaldehyde and propane in the air [25]. However, as will be seen later, this behavior is not always verified. From above results, it can be seen that FST-5 have the best catalytic activity of all synthesized catalysts. For this reason, its efficacy has been tested in the degradation of the herbicide Metsulfuron-methyl (M. methyl) present in a commercial formula.

3.6.2 Effect of FST-5 amount on the photodegradation of Metsulfuron-methyl

As can be seen in Figure 11, the decomposition rate of this herbicide increases with the amount of FST-5 up to a ratio of 2.5 g L^{-1}. At this point the concentration of the herbicide is significantly reduced to one-third of its starting value; above a load of 2.5 g L^{-1} the photodegradation rate does not vary, because an effect of scattering of radiation begins to take place [26]. The amount of efficient active sites is decreased by an excess of catalyst particles so that the catalyst activity stabilizes at this limit load and tends to decrease. It should be noted that in the conditions tested, M. methyl is not photolyzed in the absence of FTS-5. However, this herbicide can undergo photolysis at longer irradiation times [27].

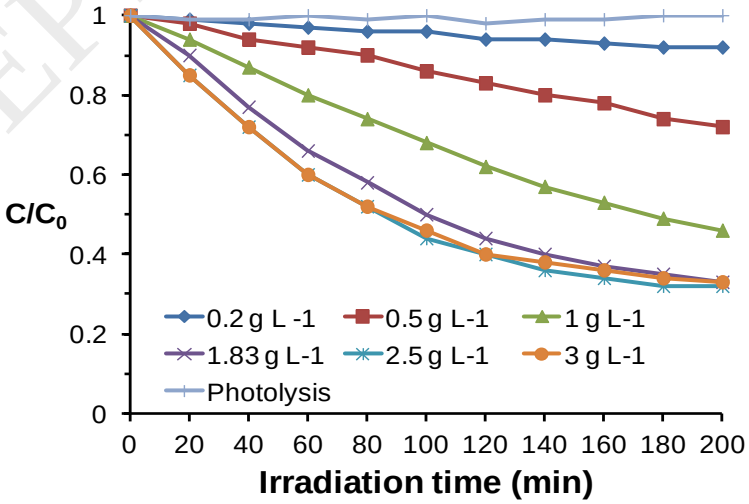

Fig. 11. Effect of the amount of FST-5 catalyst on the photocatalytic decomposition of Metsulfuron-methyl. The reaction medium has a pH value of 6.

3.6.3 Initial pH of the reaction medium

The stability of the sulfonylureas depends significantly on the pH of the aqueous medium in which they are present. In acid watercourses it is easily hydrolyzed but in neutral or basic aqueous media it is resistant to hydrolysis and becomes more persistent in the environment. This is because their sulfonyl group (-SO_2-) significantly increases the acidity of the proton of the adjacent nitrogen atom. Deprotonation markedly deactivates the sulfonylureas for hydrolysis because the resulting negative charge is distributed through the sulfonylurea group, thus reducing the electrophilicity of the carbonyl group [28] and hence the attack of a water molecule. On the contrary, if the aqueous medium is acidic enough (pH <6), this herbicide is protonated and this protective effect is not observed.

M. methyl is not hydrolyzed in a pH range of 6-9 [28] since it has a pKa equal to 3.3 [29]. For this reason, the effectiveness of FST-5 under these conditions has been evaluated and the results are presented in Figure 12. As the pH increases, the concentration of OH^- anions is greater and therefore more OH• radicals can be generated on the catalyst surface. However, since the isoelectric point of FST-5 is ca. 5.4, the negative charge on the TiO_2 surface also increases, which increases the electrostatic repulsion with the anion of the herbicide and thus the photodegradation of M. methyl decreases.

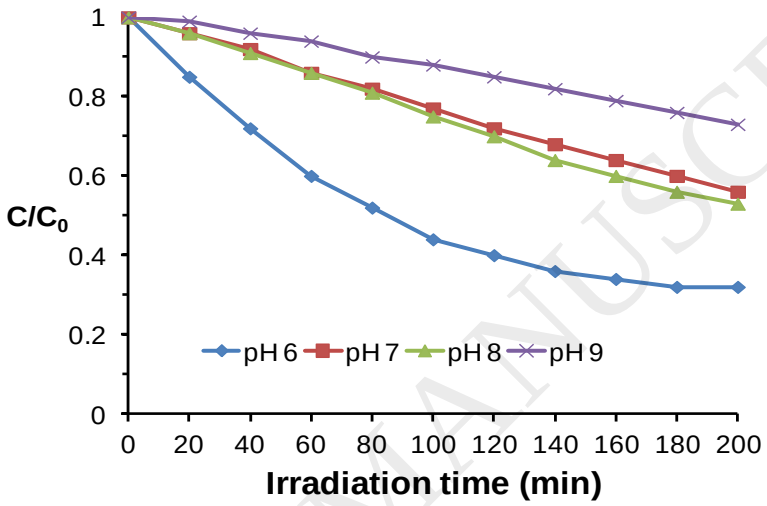

Fig. 12. Photodegradation of Metsulfuron-methyl at different pH values. [FST-5] = 2.5 g L^{-1}.

Based on these results it can be seen that 6 is the optimum pH value for degradation of M. methyl under the conditions tested. This pH is found in most natural watercourses.

3.6.5 FST-5 vs unsupported TiO_2

The activity of FST-5 was compared with the activities of equivalent amounts (47.4% according to Table 3) of two unsupported TiO_2 samples. One of them was synthesized according to the sol-gel technique, and the other sample was P25. The results can be observed in Figure 13. FST-5 possess similar activity to synthesized TiO_2, possibly due to the similar active surface area between them. Since the pH of the M. methyl solution is 6, and the isoelectric point of the unsupported TiO_2 is 5.1, the TiO_2 particles are negatively charged and do not agglomerate, thus presenting the largest possible active surface.

The significative difference between the activity of the synthesized TiO_2 and that of P25 is also observed, and this may be due to several factors. One of them is the difference between isoelectric points of both samples, since for P25 this value is 6.25 [26b], therefore in the reaction medium it is positively charged and attracts the anions of the herbicide. The opposite effect can be observed with the synthesized TiO_2, which partially repels the above-mentioned anions.

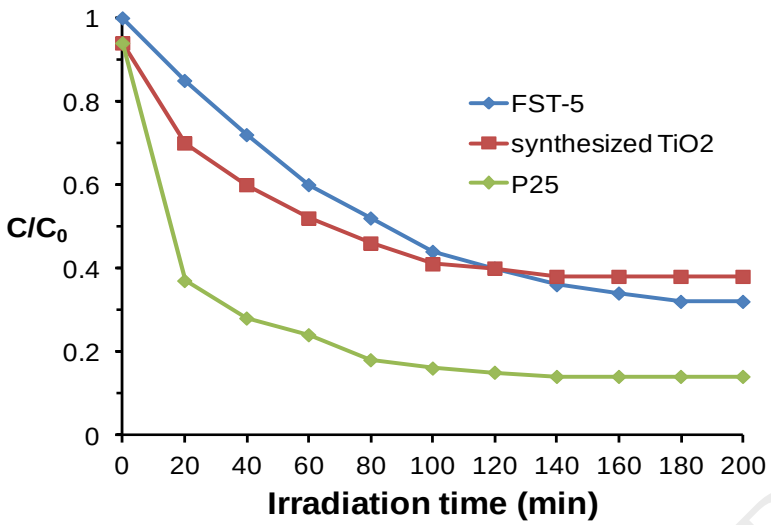

Fig. 13. Photocatalytic degradation of Metsulfuron-methyl on FST-5 and an equivalent mass of sol-gel synthesized TiO_2 and P25. [FST-5] = 2.5 g L^{-1}; [synthesized TiO_2] = [P25] = 1.186 g L^{-1}.

Another factor to consider is the crystalline composition of both catalyst samples: the synthesized TiO_2 consists of 71% anatase and 29% brookite, while the P25 composition is 75% anatase and 25% rutile. Under certain reaction conditions, it has been found that the activity of TiO_2 with a composition similar to the first of those mentioned is lower than that corresponding to P25 due to its lower photon efficiency [30]. It should also be considered that, although some authors indicate that the optimal effective amount of brookite would oscillate between 20 and 40 %, the behavior of anatase-brookite compounds depends significantly on many other factors such as specific surface area, the degree of crystallinity, crystal sizes of different phases, surface hydroxylation and synthesis method [25]. Although the activity of P25 is greater than that of FST-5, the latter can easily be removed from the reaction medium, unlike the commercial product.

3.6.6 Comparison between artificial and solar photocatalytic decomposition of Metsulfuron-methyl

If a catalyst is active under solar irradiation it would allow us to avoid the use of artificial sources of radiation, reducing operating costs and expanding its use to areas away from urban centers. The city of Salta registers Ultraviolet Indices within the ranges Very High (8-10) and Extreme (11 or more) during summer and fall seasons. February is the month which the highest values of total ultraviolet radiation are recorded [31] and for this reason, this month was chosen to carry out the solar photocatalysis experiments at noon hours. The results obtained in comparison with the laboratory tests are shown in Figure 14.

Under solar radiation FST-5 showed lower activity than that registered with the UV lamp, decreasing the concentration of M. methyl up to 70% of its initial value. This difference is based on the lower intensity of total solar UV radiation, estimated between 0.25 and 0.30 W m^{-2} [31] compared to the corresponding UV lamp, whose total value is 7.3 W m^{-2} (UVA + UVB). As it is known, the efficiency in the photocatalytic degradation of a contaminant is increased with the intensity of UV radiation [32]. However, FST-5 could be used as a solar pretreatment method to reduce the initial concentration of this herbicide (and possibly other organic pollutants) in aqueous media, thus reducing the time of subsequent treatment with artificial UV sources and thereby the energy cost. Also, this herbicide does not photolyze when it is exposed to solar radiation without FST-5, with a slight increase in its concentration by water evaporation.

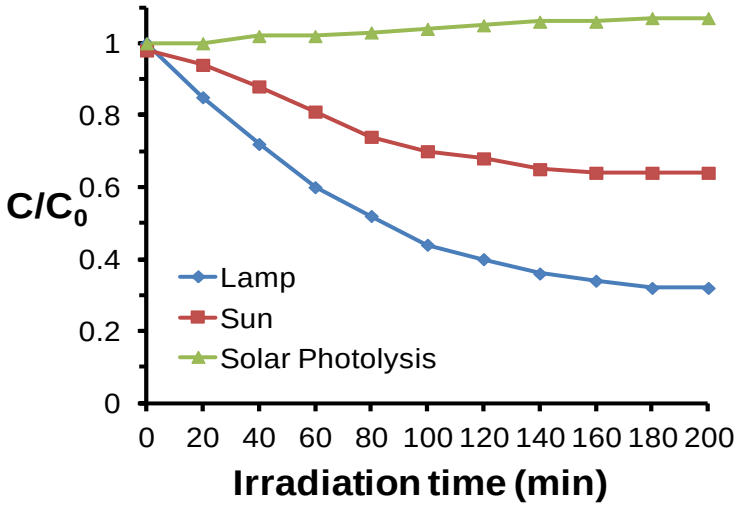

Fig. 14. Solar and artificial photodegradation of Metsulfuron-methyl with FST-5. This herbicide did not undergo photolysis under solar radiation. [FST-5] = 2.5 g L^{-1}.

3.6.7 Reuse of catalyst

The reuse of a photocatalyst is one of the most important parameters to determine, from an economic point of view, the application of this material in water treatment systems [33]. In Figure 15 it can be seen that during the first three cycles the catalyst loses activity, stabilizing in the last two cycles where a degradation of 30% of the initial concentration of the herbicide is finally reached. Since M. methyl solution is prepared from a commercial formulation (its composition of inert compounds is unknown), it may contain inhibitors of the TiO_2 activity present in FST-5, binding to it with each cycle. Sulfate anion, another inhibitor of TiO_2 activity, can also be formed as a byproduct of the degradation of this herbicide [34]. These would be the most important causes by which the activity of FST-5 decreases progressively.

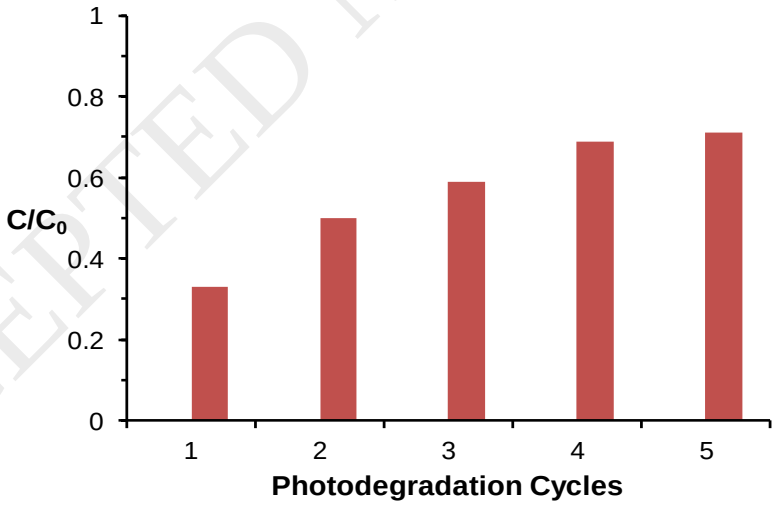

Fig. 15. Photodegradation of Metsulfuron-methyl at different cycles. [FST-5] = 2.5 g L^{-1}.

4. Conclusions

A series of magnetic photocatalysts composed of Fe_3O_4 / SiO_2 / TiO_2 were successfully synthesized at low temperature with various combinations of anatase-brookite phases. Aging time had a decisive influence on the structural properties of synthesized TiO_2: crystallinity, particle size and its related specific surface area were modified by varying this parameter. FST-5 was the best photocatalyst as a result of the optimal combination of these factors. This catalyst was efficient to significantly decrease the concentration of the herbicide Metsulfuron-methyl under conditions in which this agrochemical is persistent in an aqueous medium. Its activity was similar to the equivalent amount of TiO_2 in suspension and can be easily

removed from the reaction medium, unlike unsupported TiO_2. Under solar radiation, it is active and could be used as a decontamination pretreatment, which would decrease the total energy cost of the final process with artificial UV sources. These results are encouraging because a commercial formula of this herbicide was used in the experiments, which greatly approximated laboratory conditions to a real situation with natural watercourses.

Acknowledgements

We gratefully acknowledge Lic. Lilian Davies for her technical assistance in Raman and FTIR spectroscopy techniques.

We also thanks CONICET (Consejo Nacional de Investigaciones Científicas y Técnicas) and Consejo de Investigación from National University of Salta for their financial support.

Declarations of interest: none

References

[1] (a) A. Fujishima, T. Rao, D. Tryk, Titanium dioxide photocatalysis, J. Photochem. Photobiol. C 1 (2000) 1-21 https://doi.org/10.1016/S1389-5567(00)00002-2. (b) M. Anpo, M. Takeuchi, The design and development of highly reactive titanium oxide photocatalysts operating under visible light irradiation, J. Catal. 216 (2003) 505-516 https://doi.org/10.1016/S0021-9517(02)00104-5. (c) S. Devipriya, S. Yesodharan, Photocatalytic degradation of pesticide contaminants in water, Sol. Energy Mater. Sol. Cells 86 (2005) 309-348 https://doi.org/10.1016/j.solmat.2004.07.013. (d) N. García, F. Amat-Guerri, Photodegradation of hydroxylated N-heteroaromatic derivatives in natural-like aquatic environments: A review of kinetic data of pesticide model compounds, Chemosphere 59 (2005) 1067-1082 https://doi.org/10.1016/j.chemosphere.2004.12.028.

[2] S. Li, L. Wallis, S. Diamond, H. Ma, D. Hoff, Species sensitivity and dependence on exposure conditions impacting the phototoxicity of TiO_2 nanoparticles to benthic organisms, Environ. Toxicol. Chem. 33 (2014) 1563-1569 https://doi.org/10.1002/etc.2583.

[3] (a) R. Shukla, A. Kumar, D. Gurbani, A. Pandey, S. Singh, A. Dhawan, TiO_2 nanoparticles induce oxidative DNA damage and apoptosis in human liver cells, Nanotoxicology 7 (2013) 48-60 https://doi.org/10.3109/17435390.2011.629747. (b) S. Makumire, V. Chakravadhanula, G. Köllisch, E. Redel, A. Shonhai, Immunomodulatory activity of zinc peroxide (ZnO_2) and titanium dioxide (TiO_2) nanoparticles and their effects on DNA and protein integrity, Toxicol. Lett. 227 (2014) 56–64 https://doi.org/10.1016/j.toxlet.2014.02.027.

[4] X. Yan, K. Yuan, N. Lu, H. Xu, S. Zhang, N. Takeuchi, H. Kobayashi, R. Li, The interplay of sulfur doping and surface hydroxyl in band gap engineering: Mesoporous sulfur-doped TiO_2 coupled with magnetite as a recyclable, efficient, visible light active photocatalyst for water purification, Appl. Catal. B 218 (2017) 20–31 https://doi.org/10.1016/j.apcatb.2017.06.022.

[5] Y. Gao, B. Chen, H. Li, Y. Ma, Preparation and characterization of a magnetically separated photocatalyst and its catalytic properties, Mater.Chem.Phys. 80 (2003) 348-355 https://doi.org/10.1016/S0254-0584(02)00515-1.

[6] S. Laurent, D. Forge, M. Port, A. Roch, C. Robic, L. Vander-Elst, R. Muller, Magnetic Iron Oxide Nanoparticles: Synthesis, Stabilization, Vectorization, Physicochemical Characterizations, and Biological Applications, Chem. Rev. 108 (2008) 2064–2110 https://doi.org/10.1021/cr068445e.

[7] (a) D. Beydoun, R. Amal, G. Low, S. McEvoy, Occurrence and prevention of photodissolution at the phase junction of magnetite and titanium dioxide, J. Mol. Catal. A 180 (2002) 193-200 https://doi.org/10.1016/S1381-1169(01)00429-0. (b) F. Chen, Y. Xie, J. Zhao, G. Lu, Photocatalytic degradation of dyes on a magnetically separated photocatalyst under visible and UV irradiation, Chemosphere 44 (2001) 1159 -1168 https://doi.org/10.1016/S0045-6535(00)00277-0. (c) P.

Álvarez, J. Jaramillo, F. López-Piñero, P.K. Plucinski, Preparation and characterization of magnetic TiO_2 nanoparticles and their utilization for the degradation of emerging pollutants in water, Appl. Catal. B 100 (2010) 338–345 https://doi.org/10.1016/j.apcatb.2010.08.010.

[8] T.A. Gad-Allah, S. Kato, S. Satokawa, T. Kojima, Role of core diameter and silica content in photocatalytic activity of $TiO_2/SiO_2/Fe_3O_4$ composite, Solid State Sci. 9 (2007) 737-743 https://doi.org/10.1016/j.solidstatesciences.2007.05.012.

[9] J. Xu, Y. Ao, D. Fu, C. Yuan, Low-temperature preJ. Phys. Chem. Solidscoated magnetite, -paration of anatase titania 69 (2008) 1980-1984 https://doi.org/10.1016/j.jpcs.2008.02.015.

[10] X. Song, L. Gao, Fabrication of Bifunctional Titania/Silica-Coated Magnetic Spheres and their Photocatalytic Activities, J. Am. Ceram. Soc. 90 (2007) 4015–4019 https://doi.org/10.1111/j.1551-2916.2007.01989.x

[11] (a) S. Watson, J. Scott, D. Beydoun, R. Amal, Studies on the preparation of magnetic photocatalysts, J. Nanopart. Res. 7 (2005) 691–705 https://doi.org/10.1007/s11051-005-7520-8. (b) Q. Yuan, N. Li, W. Geng, Y. Chi, X. Li, Preparation of magnetically recoverable Fe_3O_4@SiO_2@meso-TiO_2 nanocomposites with enhanced photocatalytic ability, Mater. Res. Bull. 47 (2012) 2396-2402 https://doi.org/10.1016/j.materresbull.2012.05.031.

[12] Y. Ao, J. Xu, D. Fu, X. Shen, C. Yuan, Low temperature preparation of anatase TiO_2-coated activated carbon, Colloids Surf. A 312 (2008) 125–130 https://doi.org/10.1016/j.colsurfa.2007.06.039.

[13] (a) S.L. Tie, H.C. Lee, Y.S. Bae, M.B. Kim, K. Lee, C.H. Lee, Monodisperse Fe_3O_4/Fe@SiO_2 core/shell nanoparticles with enhanced magnetic property, Colloid Surf. A 293 (2007) 278-285 https://doi.org/10.1016/j.colsurfa.2006.07.044. (b) Y.S. Li, J.S. Church, A.L. Woodhead, F. Moussa, Preparation and characterization of silica coated iron oxide magnetic nano-particles, Spectrochim. Acta Mol. Biomol. Spectrosc. 76 (2010) 484–489 https://doi.org/10.1016/j.saa.2010.04.004.

[14] C.F. Chang, Y.L. Wu, S.S Hou, Preparation and characterization of superparamagnetic nanocomposites of aluminosilicate/silica/magnetite, Colloids Surf. A 336 (2009) 159-166 https://doi.org/10.1016/j.colsurfa.2008.11.042.

[15] K. Porkodi, S.D. Arokiamary, Synthesis and spectroscopic characterization of nanostructured anatase titania: A photocatalyst, Mater. Charact. 58 (2007) 495-503 https://doi.org/10.1016/j.matchar.2006.04.019.

[16] M. Rezaee, S.M. Mousavi Khoie, K.H. Liu, The role of brookite in mechanical activation of anatase-to-rutile transformation of nanocrystalline TiO_2: An XRD and Raman spectroscopy investigation, CrystEngComm 13 (2011) 5055-5061 https://doi.org/10.1039/c1ce05185g.

[17] M. Gopal, W.J. Moberly Chan, L.C. De Jonghe, Room temperature synthesis of crystalline metal oxides, J. Mater. Sci. 32 (1997) 6001-6008 https://doi.org/10.1023/A:1018671212890.

[18] J.P. Sanders, P.K. Gallagher, Thermomagnetometric evidence of γ-Fe_2O_3 as an intermediate in the oxidation of magnetite, Thermochim. Acta 406 (2003) 241-243 https://doi.org/10.1016/S0040-6031(03)00250-8.

[19] S.P.E. Forsmo, Oxidation of magnetite concentrated powders during storage and drying, Int. J. Miner. Process. 75 (2005) 135-144 https://doi.org/10.1016/j.minpro.2004.08.010.

[20] M. Crian, A. Brileanu, M. Rileanu, D. Crian, V. S. Teodorescu, R. Birjega, V. E. Marinescu, J. Madarász, G. Pokol, TiO2-based nanopowders obtained from different Ti-alkoxides, J. Therm. Anal. Calorim. 88 (2007) 171–176. https://doi.org/10.1007/s10973-006-8125-x

[21] N. Wetchakun, B. Incessungvorn, K. Wetchakun, S. Phanichphant, Influence of calcination temperature on anatase to rutile phase transformation in TiO_2 nanoparticles synthesized by the modified sol–gel method, Mater. Lett. 82 (2012) 195-198. https://doi.org/10.1016/j.matlet.2012.05.092.

[22] M. E. Manriquez, M. Picquart, X. Bokhimi, T. López, P. Quintana, J. M. Coronado, X-Ray Diffraction, and Raman Scattering Study of Nanostructured ZrO2-TiO2 Oxides Prepared by Sol–Gel, J. Nanosci. Nanotechnol. 8 (2008) 6623–6629. https://doi.org/10.1166/jnn.2008.041

[23] H. Zhang, J.F. Banfield, Understanding Polymorphic Phase Transformation Behavior during Growth of Nanocrystalline Aggregates: Insights from TiO_2, J. Phys. Chem. B 104 (2000) 3481-3487 https://doi.org/10.1021/jp000499j.

[24] B.K. Mutuma, G.N. Shao, W.D. Kim, H.T. Kim, Sol-gel synthesis of mesoporous anatase-brookite and anatase-brookite–rutile TiO_2 nanoparticles and their photocatalytic properties, J. Colloid Interface Sci. 442 (2015) 1-7 https://doi.org/10.1016/j.jcis.2014.11.060.

[25] A. Di Paola, M. Bellardita, L. Palmisano, Review: Brookite, the Least Known TiO_2 Photocatalyst, Catalysts 3 (2013) 36-73 https://doi.org/10.3390/catal3010036.

[26] (a) M. Huang, C. Xu, Z. Wu, Y. Huang, J. Lin, J. Wu, Photocatalytic discolorization of methyl orange solution by Pt modified TiO_2 loaded on natural zeolite, Dyes Pigm. 77 (2008) 327-334 https://doi.org/10.1016/j.dyepig.2007.01.026. (b) S. Ahmed, M. Rasul, R. Brown, M. Hashib, Influence of parameters on the heterogeneous photocatalytic degradation of pesticides and phenolic contaminants in wastewater: A short review, J. Environ. Manage. 92 (2011) 311-330 https://doi.org/10.1016/j.jenvman.2010.08.028.

[27] S. Samanta, R.K. Kole, A. Chowdhury, Photodegradation of Metsulfuron methyl in aqueous solution, Chemosphere 39 (1999) 873-879.

[28] A.K. Sarmah, J. Sabadie, Hydrolysis of Sulfonylurea Herbicides in Soils and Aqueous Solutions: a Review, J. Agric. Food Chem. 50 (2002) 6253-6265 https://doi.org/10.1021/jf025575p.

[29] S. Trapp, Bioaccumulation of Polar and Ionizable Compounds in Plants, in: J. Devillers (Ed.), Ecotoxicology Modeling, Springer US, New York, 2009, pp. 299-353 https://doi.org/10.1007/978-1-4419-0197-2.

[30] A.A. Ismail, T.A. Kandiel, D.W. Bahnemann, Novel (and better?) titania-based photocatalysts: Brookite nanorods and mesoporous structures, J. Photochem. Photobiol. A 216 (2010) 183–193 https://doi.org/10.1016/j.jphotochem.2010.05.016.

[31] M. Utrillas, M. Marín, A. Esteve, G. Salazar, H. Suarez, J. Castillo, J. Martínez-Lozano, UVER and UV index at high altitude in Northwestern Argentina, J. Photochem. Photobiol. B 163 (2016) 290–295 https://doi.org/10.1016/j.jphotobiol.2016.08.012.

[32] H. Zangeneh, A. Zinatizadeh, M. Habibi, M. Akia, M. Hasnain Isa, Photocatalytic oxidation of organic dyes and pollutants in wastewater using different modified titanium dioxides: A comparative review, J. Ind. Eng. Chem. 26 (2015) 1-36 https://doi.org/10.1016/j.jiec.2014.10.043.

[33] A. Hamdi, A. Ferraria, A. Botelho do Rego, D. Ferreira, D. Conceicão, L. Vieira Ferreira, S. Bouattour, Bi–Y doped and co-doped TiO_2 nanoparticles: Characterization and photocatalytic activity under visible light irradiation, J. Mol. Catal. A: Chem. 380 (2013) 34–42 https://doi.org/10.1016/j.molcata.2013.09.005.

[34] S. Rafqah, P. Wong-Wah-Chung, A. Aamili, M. Sarakha, Degradation of metsulfuron methyl by heterogeneous photocatalysis on TiO_2 in aqueous suspensions: Kinetic and analytical studies, J. Mol. Catal. A: Chem. 237 (2005) 50-59 https://doi.org/10.1016/j.molcata.2005.03.044.